

Isotherms, kinetics and thermodynamics for adsorption of pyridine vapors on modified activated carbons

Rashmi Dhawan · K. K. Bhasin · Meenakshi Goyal

Received: 14 May 2014/Revised: 12 September 2014/Accepted: 12 January 2015/Published online: 25 January 2015
© Springer Science+Business Media New York 2015

Abstract The adsorption isotherms of pyridine have been determined gravimetrically on different samples of granulated, fibrous and spherical activated carbons. Several chemical treatments such as oxidation, degassing and impregnation have been carried out on as-received activated carbon cloth (ACC) so as to modify the surface characteristics of the activated carbon. The porous and chemical structure of modified and unmodified activated carbons has been characterised by XRD, TGA–DTG, SEM and pore size distribution techniques. The adsorption increases on oxidation while decreases on degassing which can be correlated to increase and decrease in the concentration of surface oxygen groups. Loading with Ag^+ and Cu^{2+} increases the adsorption of pyridine compared with the unloaded sample while loading with Cr^{6+} decreases the adsorption of these vapors. The adsorption–desorption branches of pyridine vapors on metal impregnated do not meet even at zero relative vapor pressure indicating the chemisorption or other specific interactions. The adsorption kinetics data has been examined using the linear driving force and empirical diffusion models. The initial decrease in isosteric enthalpy of adsorption for modified and unmodified ACC indicates the effect of surface heterogeneity and later increase indicates the influence of lateral

interactions between adsorbate molecules. The results suggest that the adsorption of pyridine involves the physisorption as well as specific interactions with carbon oxygen functional groups and metal complexes present on the carbon surface.

Keywords Activated carbon adsorption · Surface functional groups · Metal impregnation · Adsorption kinetics · Isosteric enthalpy of adsorption

1 Introduction

Pyridine is widely used as building blocks in many agrochemicals and pharmaceuticals (ATSDR 1992) and as solvent and chemical intermediate in organic synthesis. Pyridine and pyridine-containing compounds are present throughout the environment at very low levels. Pyridine has been found in the air inside and around factories that produce it or use it to make other products. Pyridine is also released into the air from burning cigarettes and from hot coffee. Effects of acute pyridine intoxication include dizziness, headache, nausea and anorexia. Further symptoms include abdominal pain, pulmonary congestion, neurological and renal effects (ATSDR 1992; ATSDR 2008). Currently it is evaluated as a possible carcinogenic agent (ATSDR 2008). The Occupational Safety and Health Administration (OSHA) has set an average air exposure level of 5 ppm for an 8-h day, 40-h work week while the National Institute for Occupational Safety and Health (NIOSH) has set 3,600 ppm in air as the level that is immediately dangerous to life and health.

Adsorption of pyridine vapors has been studied by various researchers on different types of adsorbents such as silica, zeolites and activated carbons. The heat of adsorption studies (Muminov 2003) of pyridine vapors on

R. Dhawan (✉) · K. K. Bhasin
Department of Chemistry, Panjab University, Chandigarh, India
e-mail: rashu.v3@gmail.com

R. Dhawan
Sri Guru Teg Bahadur Khalsa College,
Anandpur Sahib 140118, India

M. Goyal
Dr. S.S. Bhatnagar University Institute of Chemical Engineering
& Technology, Panjab University, Chandigarh, India

dehydrated microporous clay with intercalated polyhydroxyaluminium cations showed that the transformation of polyhydroxyaluminium cations upon thermal treatment of intercalated clays diminishes the pore size and decreases the adsorption enthalpy of pyridine. However, the heats of adsorption of pyridine on silica were found to be decreased with heterogeneity of the surface (Bakaev et al. 2007). The influence of surface properties of activated carbons prepared by gasification with different gases on adsorption of pyridine showed that the adsorption of pyridine was related to the chemistry of the carbon surface rather than the surface area or the total pore volume (Attia 1997). Also, the influence of changes in the surface properties and pore structure was studied on the adsorption of pyridine vapors by substituting the Na^+ ions of natural montmorillonite clay. The sorption follows mechanism of pore volume filling (Muminov et al. 2004; Muminov and Gulyamova 2004). The adsorption behavior of pyridine vapor on WK11 ion exchange resin indicated that pyridine could disrupt weak H bonds of original WK11 to form a strong pyridine-COOH hydrogen bond (Chen et al. 2004). While the adsorption of pyridine on activated carbons involved physisorption on the oxygen free surface and chemisorption on acidic carbon-oxygen groups (El-Nabarawy and Petro 1997). Rate constants, activation energies and compensation effects indicated that the adsorption involved diffusion barrier at the pore entrance (Yuzak et al. 2001).

The above brief perusal of the literature shows that very little work has been carried out for adsorption of pyridine especially on metal impregnated carbons. Furthermore, no integrated approach regarding the variation in surface area, chemical structure and the polarity of the carbon surface as well as the polarity of the adsorbate on the adsorption of pyridine has been made. Very little information is available on the kinetic and thermodynamic data which is essential to design the adsorption systems for the removal of these compounds. The present work discusses the mechanism of the adsorption of pyridine based on the adsorption isotherms, adsorption kinetics and the isosteric enthalpies of adsorption on unmodified and modified activated carbons. In this paper, for the first time, we have calculated the % contribution of polar-polar and dispersion interactions involved in the adsorption of these compounds using the empirical diffusion model.

2 Materials and methods

2.1 Materials

Two samples of granulated activated carbons GAC-1240 and GAC-R obtained from Norit N. V. Netherlands, a sample of activated carbon fiber ACF-307 obtained from

Ashland Petroleum Company of USA and a sample of activated carbon cloth (ACC) and a sample of spherical activated carbon (SAC) obtained from HEG Ltd., Bhopal, India, have been used as adsorbents in these studies. These samples are referred to as 'as-received' activated carbons in the text. In order to modify the surface chemistry of the carbon surface, two of the carbon samples were oxidized with nitric acid, ammonium persulphate and hydrogen peroxide in the solution phase. The nitric acid oxidized samples were also degassed at 400, 650 and 950 °C to obtain samples associated with varying amounts of carbon-oxygen surface groups. The activated carbons have been also impregnated with Ag, Cu and Cr ions.

2.2 Modification of carbon samples

2.2.1 Oxidation of the activated carbons

The activated carbon samples were oxidized with nitric acid, ammonium persulphate and hydrogen peroxide. The procedures were as follows: 5.0 g of carbon was heated with 200 ml of 50 % nitric acid at 353 K until 10 ml of the acid was left. The carbon sample was then washed exhaustively with hot distilled water so as to remove the remaining nitrates. The treatment with ammonium persulphate was carried out with 5.0 g carbon per 200 ml of a saturated solution of this salt in sulphuric acid (1 M) at 298 K for 48 h. The contents were shaken in a mechanical shaker for about 48 h and then filtered. The oxidized carbon sample was washed with distilled water until free of sulphate ions. The oxidation with hydrogen peroxide was done by shaking 5.0 g of carbon sample mixed with 200 ml of concentrated H_2O_2 (9.8 M) at 298 K in mechanical shaker for 48 h. The oxidized samples were then dried in an electric oven at 120 °C.

2.2.2 Degassing of the carbons

The oxidized carbons were degassed at temperatures of 400, 650 and 950 °C to eliminate varying amounts of the carbon-oxygen surface groups. The degassing was carried out by placing 5.0 g of the carbon sample in a temperature controlled tube furnace. The tube furnace was then connected to a Hyvac Cenco vacuum pump capable of giving vacuum to the order of 3×10^{-3} mm of Hg. Temperature of the tube furnace was set to the appropriate level by applying a suitable voltage. After degassing at each temperature, the sample was allowed to cool in vacuum to avoid reformation of the carbon-oxygen surface groups. The cooled sample was then transferred to a stoppered bottle flushed with nitrogen. These samples are referred to as 'degassed samples' in the text.

2.2.3 Impregnation of activated carbon

Impregnation of Cr(VI), Cu(II) and Ag(I) has been carried out by placing dried 1.0 g ACC sample in contact with 100 ml of potassium dichromate solution, copper nitrate solution, silver nitrate solution, each having concentration of 500 ppm. The suspensions were placed in a thermostat at 303 K for 48 h with occasional shaking and a blank was also placed for this solution. Amount of Cu(II) and Cr(VI) impregnated into the carbon was estimated by titration against standard sodium thiosulphate solution while amount of Ag(I) impregnated in activated carbon was estimated by titration against standard NaCl solution (0.01 M) using 5 % potassium chromate (K_2CrO_4) as indicator. These samples are referred to as ‘impregnated samples’ in the text.

2.3 Characterization of carbon samples

2.3.1 High temperature evacuation

The carbon–oxygen surface groups present on the as-received, oxidized and degassed carbon samples were determined by evacuating 1.0 g portion of each sample at gradually increasing temperatures up to 950 °C. The carbon sample contained in a platinum boat was placed in a tube furnace. The temperature of the furnace was allowed to rise gradually in steps of 50 °C to ensure complete elimination of the gas at the previous temperature. The carbon–oxygen surface groups decompose into CO_2 , CO and water vapor which were measured using usual analytical procedures. (Bansal et al. 1978; Puri and Bansal, 1964).

2.3.2 Base neutralisation capacity (surface acidity)

Surface acidity of activated carbon was determined by mixing 1.0 g of each carbon sample (oven dried at 120 °C) with 100 ml of 0.1 N sodium hydroxide solution, shaking the suspension for 48 h and titrating the aliquot of clear supernatant liquid against a standard acid solution (0.1 N HCl) (Bansal et al. 1978; Puri and Sharma 1970).

2.3.3 Elemental analysis

C, H, N and O contents of the as-received carbon samples were determined by using Perkin Elmer 2400 CHN elemental analyzer. Nitrogen, carbon and hydrogen contents were determined directly while the oxygen content was calculated by difference.

2.3.4 BET surface area and pore size distribution

BET surface area, pore volume, pore size distribution and pore radius have been determined by nitrogen adsorption–

desorption at 77 K in relative vapor pressure range 0.002–0.99 using quadrawin software provided with Quatachrome Nova 2200e surface area analyser. The surface area was calculated using the BET method while the total pore volume was directly calculated from the volume of nitrogen adsorbed at the highest relative vapor pressure $p/p_0 = 0.99$. Micropore volume was calculated using the Dubinin–Radushkevich (DR) equation and the pore size by Dubinin–Astakov (DA) method.

2.3.5 Powder XRD diffraction studies

Powder XRD patterns were obtained on a X’pert PRO diffractometer equipped with a copper target ($Cu K_\alpha$ radiation, $\lambda = 1.54060 \text{ \AA}$), a crystal graphite monochromator and a scintillation detector. The instrument was run at 45 kV and 40 mA by step-scanning from 5° to 70° 2θ in increments of 0.017° 2θ with a counting time of 20 s for each step. The operation was carried out at 25 °C and atmospheric pressure.

2.3.6 Scanning electron microscopy (SEM)

Scanning Electron Micrographs were measured using Hitachi S-4300 model at an accelerating voltage of 10 kV to visualise the surface morphology and structure of commercial and modified ACC. Before observation, the samples were dried and then metallized with a thin layer of Au in a Fine Coat Ion Sputter (JFC 6100). Observations were carried out at magnifications ranging from 500 to 10,000.

2.3.7 Thermogravimetric analysis (TGA)

The effect of temperature on as-received and metal impregnated samples was studied by means of thermogravimetry (TG) and differential thermogravimetry (DTG) using a Perkin Elmer STA 6000 (Simultaneous thermal analyzer) instrument. Known amount (30 mg) of the activated carbon samples was put in a crucible and was heated at a ramping rate of 10 °C/min from 45 to 1,000 °C under nitrogen flow of 19 ml/min. The change in the mass of the sample with the rise in temperature was recorded by a photocell. The output of the photocell was amplified and measured continuously and precisely by recording the current through an automatic recorder. From the TG curves, DTG curves were derived.

2.4 Adsorption of pyridine vapors

Adsorption of pyridine vapors was measured using a quartz spring balance (sensitivity 20.9 cm/g) obtained from M/S Thermal Syndicate Ltd., England. The carbon sample (~50 mg) was placed in a quartz boat (also obtained from M/S Thermal Syndicate) which was suspended in a borosil

reactor. The whole system was housed in an air thermostat maintained at the required temperature. The reactor was connected to a vacuum system and a manometer. The carbon sample was evacuated under a vacuum of 10^{-4} Torr and a certain dose of the adsorbate vapors was introduced into the reactor. Preliminary experiments showed that 30 min was sufficient to attain the adsorption equilibrium. After this period, the extension of quartz spring was measured with the help of a cathetometer which could read up to 0.01 mm and the equilibrium vapor pressure was noted on the manometer. Similar more doses of the vapor were introduced into the reactor and both the extension and the equilibrium pressure were determined after each equilibrium. (Bansal et al. 1980).

3 Results and discussion

3.1 Adsorbent characterization

3.1.1 Pore characterization

The porous structural parameters such as surface area, total pore volume, micropore volume and average pore radius and DA pore radius of fibrous, granulated and SACs as deduced from the nitrogen adsorption–desorption isotherms are presented in Table 1. The data shows that the granulated carbons have higher surface area as compared with fibrous activated carbons, the surface area being maximum for SAC. It can be seen from Fig. 1 that the region between $r = 0.27$ nm and $r = 1$ nm is the most representative pore size interval of all the carbons except for ACF-307 which mainly consists of pores ranging from $r = 0.6$ nm to $r = 1.5$ nm. The location of peak maxima for ACC, GAC-R, GAC-1240 and SAC indicates the greatest proportion of pores with radius of around 0.5 nm while for ACF-307, the peak maxima is around 0.8 nm. The pore size distribution is in the range of pore radius below 2 nm. A small proportion of pores, however, show slightly large size. The ratio of the micropore volume to the total pore volume (V_m/V_t), which represents the degree of microporosity, has been found to be appreciably higher,

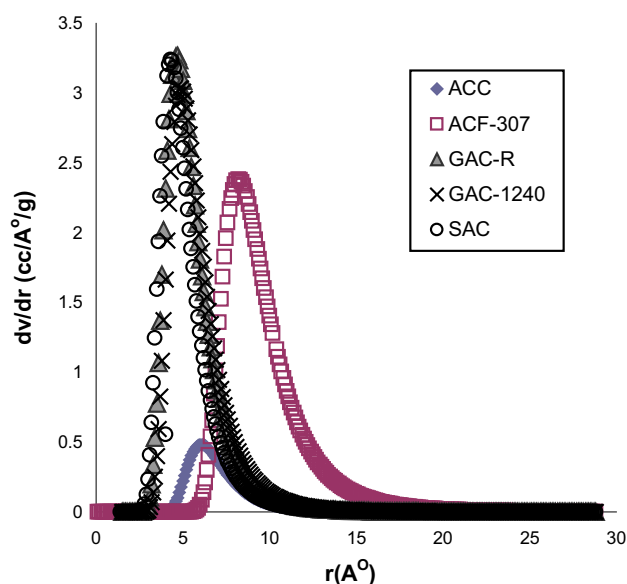


Fig. 1 Pore size distribution curves for as-received activated carbons using nitrogen adsorption isotherms

ranging from 95 to 98 % for all the carbon samples. Thus, pore size distribution curves (cf. Figure 1) and Table 1 shows that all activated carbon samples are microporous.

3.1.2 Surface chemistry

Some of the surface characteristics such as surface acidity, elemental analysis and the gases evolved on degassing at 950 °C for the activated carbons used in these investigations are given in Table 2. It is evident from the Table that the surface acidity is almost exactly equivalent to the amount of CO_2 evolved on degassing when expressed in similar units given in parentheses. This indicates that the surface groups which are evolved as CO_2 on degassing are the same as are neutralized by sodium hydroxide. It is seen that the fibrous activated carbons are associated with larger amounts of associated oxygen as compared to the granular activated carbons, the surface acidity being maximum for the ACC sample. Furthermore, the total amount of oxygen evolved as CO_2 , CO and H_2O on degassing by the decomposition of carbon–oxygen surface groups is roughly

Table 1 Porous structural parameters of different as-received activated carbons

Carbon sample	BET (N_2) surface area (m^2/g)	Total pore volume V_t (cm^3/g)	Micropore volume V_m (cm^3/g)	V_m/V_t	Average pore radius (nm)	DA pore radius (nm)
ACC	756	0.463	0.441	95.0	1.22	0.61
ACF-307	921	0.582	0.560	96.0	1.26	0.82
GAC-R	1,118	0.648	0.632	97.5	1.16	0.47
GAC-1240	1,163	0.670	0.647	96.5	1.15	0.49
SAC	1,182	0.685	0.656	95.7	1.16	0.43

Table 2 Characteristics of different as-received activated carbons

Carbon sample	Surface acidity (mEq/100 g)	Oxygen evolved (g/100 g) on degassing at 950° as				Elemental analysis (wt%)			
		CO ₂	CO	H ₂ O	Total	C	H	N	O (by diff.)
ACC	125	1.92 (120) ^a	3.15	1.31	6.38	92.56	0.92	Traces	6.52
ACF-307	98	1.56 (96) ^a	3.30	1.30	6.16	92.91	0.97	Traces	6.12
GAC-R	35	0.51 (32) ^a	1.52	1.32	3.35	95.28	0.53	Traces	4.19
GAC-1240	29	0.42 (26) ^a	1.32	1.24	2.98	96.31	0.46	Traces	3.23
SAC	16	0.31 (19) ^a	1.21	1.34	2.86	96.44	0.57	Traces	2.99

^a The values in parenthesis are the milliequivalents of CO₂ evolved on degassing

of the same order as that obtained by elemental analysis. The small differences between the two values can be attributed to the two entirely different methods used. Furthermore, as the oxygen content was determined by difference in the elemental analysis, there can be small error due to presence of trace elements.

3.2 Adsorption isotherms

The adsorption isotherms of pyridine vapors on the two samples of granulated activated carbons (GAC-1240 and GAC-R), a sample of activated carbon fiber (ACF-307), a sample of ACC and a sample of SAC are measured at 303 K and are presented in Fig. 2. All activated carbons adsorb appreciable amounts of pyridine vapors. The adsorption isotherms are Type I of the BET classification showing a sharp rise in adsorption at lower relative vapor pressures and tending to become more or less constant at higher relative pressures. The amount adsorbed generally increases with increase in surface area but there is no direct relationship between the amount adsorbed and the surface area. The adsorption data for these vapors has been analysed using Langmuir adsorption isotherm equation.

$$\frac{p}{x} = \frac{1}{x_m k} + \frac{p}{x_m}$$

The adsorption for pyridine obeys Langmuir equation. The monolayer capacity x_m obtained from these linear plots (Fig. 3) was used to calculate the surface area occupied by these molecules using 0.38 nm² as the molecular area for pyridine. The x_m values along with the BET surface area are given in Table 3. It is interesting to note that only a part of the carbon surface varying between 44 and 60 % is occupied by these molecules. This indicates that the adsorption takes place on certain specific sites on the carbon surface provided by carbon–oxygen surface groups.

3.3 Influence of surface functional groups

It is well known that almost all activated carbons are associated with appreciable amounts of chemisorbed

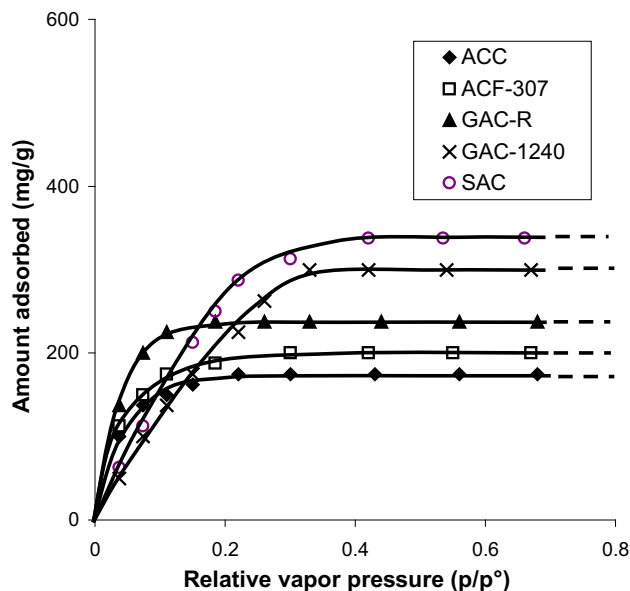


Fig. 2 Adsorption isotherms of pyridine vapors on as-received activated carbons

oxygen and the amount of chemisorbed oxygen is varied with the treatment, which the carbon was subjected to during its preparation. The chemisorbed oxygen is present on the carbon surface in the form of two types of surface groups: one which are evolved on evacuation as CO₂ in the temperature range 250–600 °C. These surface groups are acidic in character and have been identified as carboxyls and lactones. The other carbon–oxygen surface groups are evolved as CO on degassing in the temperature range 600–950 °C. These surface groups are non-acidic and have been postulated to be quinones and tend to make the carbon surface hydrophobic (Bansal et al. 1978, 1988). The amounts of both these types of surface groups are enhanced by the oxidation of the carbon surface and decreases on degassing at temperature range between 300 and 950 °C (cf. Table 4).

The influence of carbon–oxygen surface functional groups on the adsorption of pyridine was investigated by studying the adsorption isotherms on the oxidized ACC and

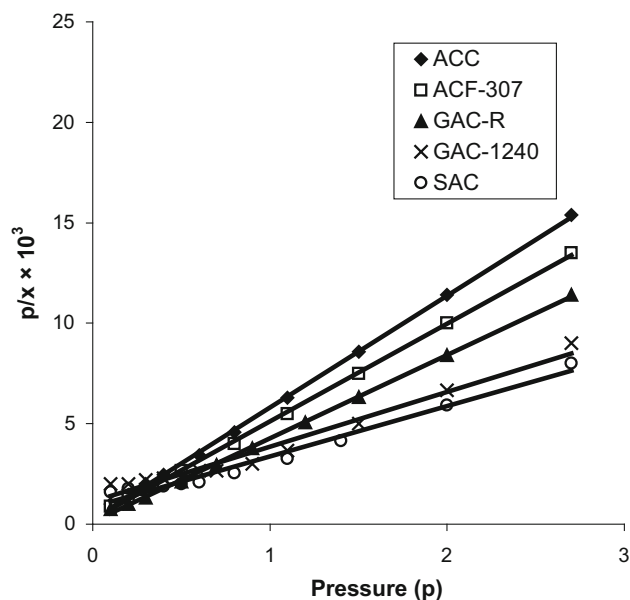


Fig. 3 Linear Langmuir plots for the adsorption of pyridine vapors on as-received activated carbons

Table 3 Surface area occupied by pyridine molecules

Carbon sample	BET (N ₂) surface area (m ² /g)	Pyridine	
		x _m (mg/g)	Surface area occupied by molecules (m ² /g)
ACC	756	180	367
ACF-307	921	206	418
GAC-R	1,118	241	492
GAC-1240	1,163	317	647
SAC	1,182	348	710

GAC-1240 carbon samples. In this paper, the curves for ACC samples are shown only (Fig. 4). It is evident that each oxidative treatment results in an appreciable increase in the adsorption depending on the nature of oxidative treatment. The increase in adsorption is maximum in case of oxidation with HNO₃ which incidentally results in the fixation of maximum amount of acidic oxygen groups that

Table 4 Surface acidity and carbon–oxygen surface groups evolved on degassing different oxidized ACC samples at 950 °C

Carbon sample	Surface acidity (mEq/100 g)	Oxygen evolved (g/100 g) as			
		CO ₂	CO	H ₂ O	Total
As-received	125	1.92 (120)	3.15	1.31	6.38
HNO ₃ -oxidized	370	6.53 (393)	7.52	1.29	15.34
(NH ₄) ₂ S ₂ O ₈ -oxidized	208	3.29 (206)	6.91	1.34	11.54
H ₂ O ₂ -oxidized	172	2.82 (176)	6.41	1.23	10.46
400°-degassed	318	5.34 (331)	7.21	1.22	13.77
650°-degassed	75	1.39 (86)	6.04	1.23	8.66
950°-degassed	Traces	Traces	Traces	Traces	Traces

are evolved as CO₂ on degassing (cf. Table 4). In order to examine whether it is the total oxygen or the acidic carbon oxygen surface groups which enhance the adsorption of these molecules, the nitric acid oxidized samples were degassed at gradually increasing temperatures of 400, 650 and 950 °C, to eliminate varying amounts of the carbon–oxygen surface groups (Puri and Bansal 1964). The adsorption isotherms on the degassed ACC samples are presented in Fig. 5. It is seen that the adsorption of pyridine decreases gradually as the temperature of degassing is enhanced. It is interesting to note that the decrease in the adsorption is only small in the case of the sample degassed at 400 °C which has lost only a small amount of the acidic surface groups retaining the non-acidic surface groups almost completely. The decrease in adsorption, however, is considerably large on the 650°-degassed carbon sample which has lost a larger part (~85 %) of the acidic surface groups although it has retained most of the non-acidic surface groups intact (cf Table 4). In case of samples outgassed at 950 °C, the adsorption of these vapors is even smaller. These samples are almost completely free of any oxygen groups and are completely hydrophobic. This shows that the increase or decrease in adsorption is determined by the amount of acidic surface groups present on the carbon surface. These acidic surface groups are polar in character and are, therefore, involved in the polar interactions with the polar adsorbate molecules. Their elimination on degassing decreases these interactions. Furthermore, increase in the amount of carbon–oxygen groups enhances acidic centres of carbon and facilitates the Lewis acid–base type interactions between the acidic sites and basic structure of pyridine molecules. On degassing, these acid–base type interactions decrease due to decrease in the acidic sites.

Since pyridine is an aromatic compound, their adsorption by activated carbons may also involve dispersive interactions between the Π electrons of the graphene layers of the carbons and Π electrons of pyridine. Thus it appears that the adsorption of pyridine on activated carbons takes place partly by dispersive and partly by polar interactions. The presence of oxygen in the carbons will reduce the

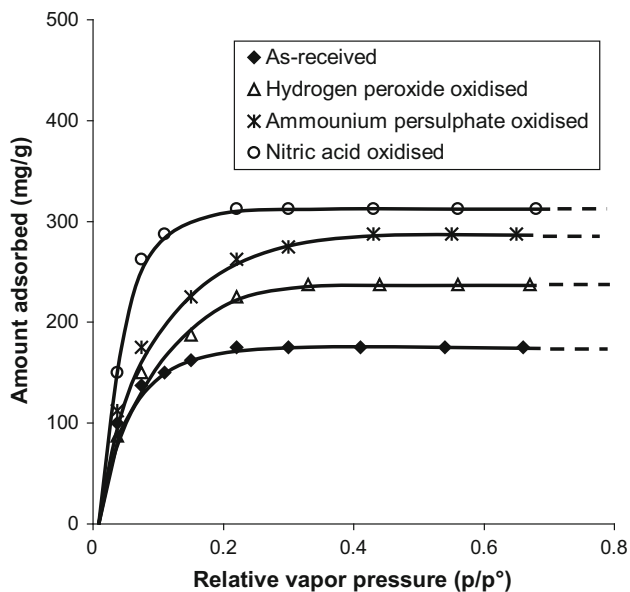


Fig. 4 Adsorption isotherms of pyridine vapors on ACC sample before and after oxidation

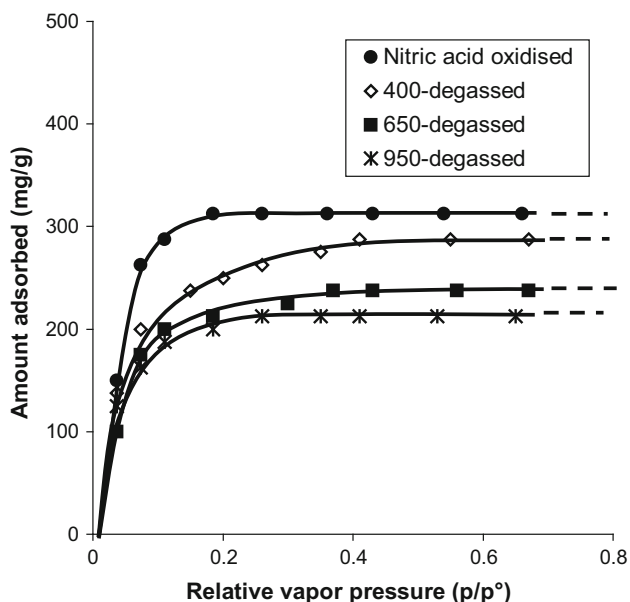


Fig. 5 Adsorption isotherms of pyridine vapors on HNO₃-oxidised ACC sample before and after degassing

dispersive interactions by decreasing the electron density due to localization or withdrawal of electrons in the graphene layers while it will enhance the polar interactions.

3.4 Influence of metal impregnants

3.4.1 Characterisation of metal impregnated carbons

ACC sample was impregnated with Cu (0.18 wt%), Cr (0.36 wt%) and Ag (1.6 wt%). Metal impregnated carbons

were characterized by pore size distribution analysis, scanning electron microscopy (SEM), powder X-ray diffraction (XRD), TGA and DTG.

In SEM micrographs of as-received ACC samples (Fig. 6a), several longitudinal grooves are observed on the surface indicating that ACC is made up of bundles of carbon fibres that are woven into a cloth. Internally each fibre is further divided into numerous small microfibrils. SEM micrographs of metal impregnated ACC samples (cf. Figs. 6 b, c, d) show that the metals have covered the surface of the fibres as indicated by the white particles on it. These metal particles are nonuniformly distributed on the external surface of ACC fibres and these could not be seen on the surface of non-impregnated ACC fibres.

The pore size distribution curves for impregnated ACC samples are shown in Fig. 7. The curves for the as-received ACC are reproduced in this figure for an easy comparison. Average pore radius, the surface area, the total pore volume and the micropore volume is decreased after impregnation (cf. Table 5). This shows that the metal particles cause partial blocking of the entrances of pores resulting in the reduced surface area and volume of the accessible pores.

The XRD patterns for as-received and metal impregnated ACC samples are presented in Fig. 8 and structural parameters for the materials are given in Table 6. The XRD patterns of activated carbons show almost no diffraction lines but two broad peaks having diffraction maxima at diffraction angles $2\theta \sim 23^\circ$ and $2\theta \sim 43^\circ$ (Short and Walker 1963). Broad peak at $2\theta \sim 23^\circ$ represents the (002) graphitic basal plane reflection and denotes strong small angle scattering indicative of an amorphous material with high porosity. The interlayer spacing of all the carbon samples for d_{002} plane is higher than that of the graphite (0.335 nm) and indicates that all the samples contain disordered graphite microcrystallites with intracrystallite voids forming the pores. Furthermore, the weaker broader peak at 43° , indicates that the (100) and (101) peaks have merged to yield a single (10) reflection, also demonstrating a relatively higher degree of randomness in these fibres. The interlayer spacing of the activated carbon was slightly decreased with metal impregnation.

Estimates of the mean microcrystallite dimensions can be obtained by application of the Debye–Scherrer equation (Carrott and Nabais 2001).

$$L = \frac{k\lambda}{\beta \cos \theta}$$

where β is the peak width at half height corrected for instrumental broadening and k is the shape factor which depends on the lattice dimension. The k values of 0.9 and 1.84 were employed for the calculation of L_c and L_a values respectively. L_a and L_c are estimates for the stacking width and stacking height of the microcrystallites. Also the mean

Fig. 6 SEM micrographs of **a** ACC ($\times 1,200$), **b** Ag-impregnated ACC ($\times 8,000$), **c** Cu-impregnated ACC ($\times 10,000$) and **d** Cr-impregnated ACC ($\times 7,000$)

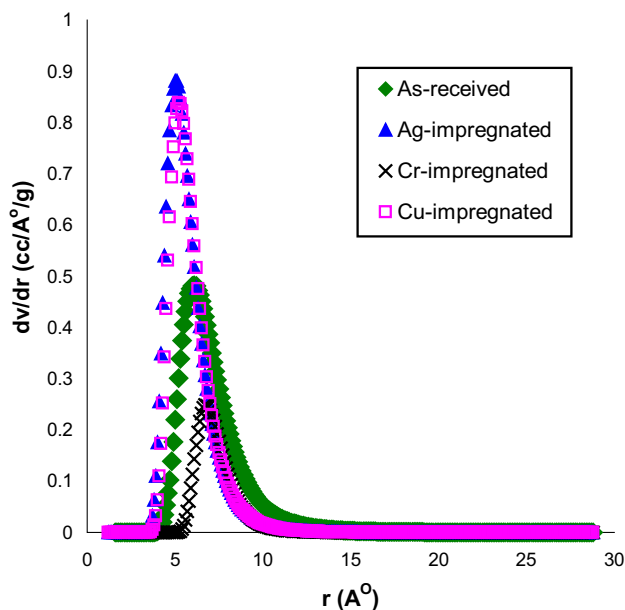
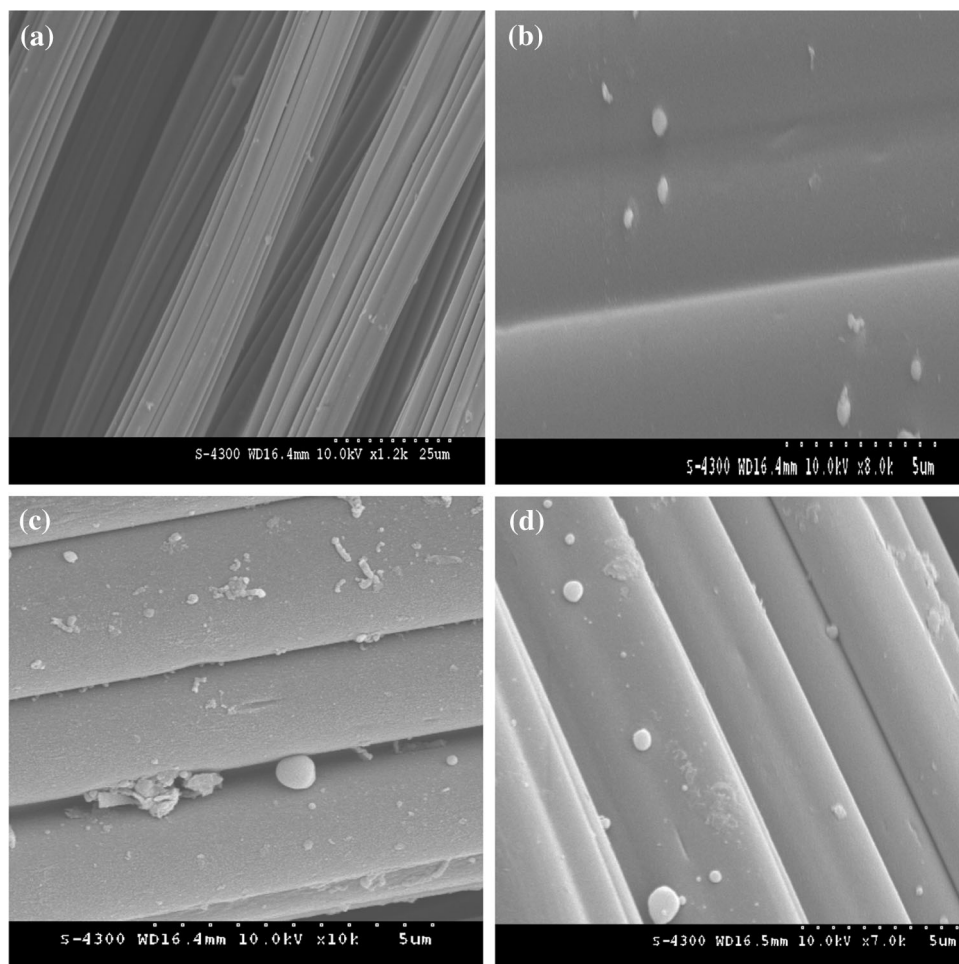


Fig. 7 Pore size distribution for as-received ACC before and after impregnation from nitrogen adsorption isotherms

number of layer planes in the microcrystallites (N_p) can be estimated using the ratio L_c/d_{002} . The wavelength (λ) of $\text{CuK}\alpha$ radiation is 0.15405 nm. The stacking height and stacking width increased slightly after impregnation. The values of L_c and L_a for typical graphitic carbon structure are 0.0670 nm and 0.2461 nm respectively.

The XRD patterns of the metal impregnated carbon samples do not show any change after loading except that the peak intensity is enhanced after each impregnation. These can be attributed to the presence of these metals on the carbon surface as amorphous material or to very small amount of metal loading on the activated carbon surface to show diffraction.

TG and DTG curves showing the thermal decomposition pattern of as-received and metal impregnated ACC samples are shown in Fig. 9a, b. TGA curves show that the weight loss occurs in three stages. The stage I of weight loss starts around 80 °C and ends around 180 °C. A gradual weight loss takes place between 200 and 600 °C and then a sudden weight loss occurs above 600 °C with a total weight loss of 33 % in case of as-received, 34 % in Cr-impregnated

Table 5 Porous structural parameters of ACC sample before and after impregnation

Carbon sample	BET(N ₂) surface area(m ² /g)	Total pore volume V _t (cm ³ /g)	Micropore volume V _{mic} (cm ³ /g)	Average pore radius (nm)
As-received	756	0.463	0.441	1.224
Cu-impregnated	670	0.351	0.323	1.047
Cr-impregnated	644	0.329	0.300	1.021
Ag-impregnated	625	0.317	0.278	1.014

Fig. 8 XRD patterns for as-received and impregnated ACC samples (Color figure online)

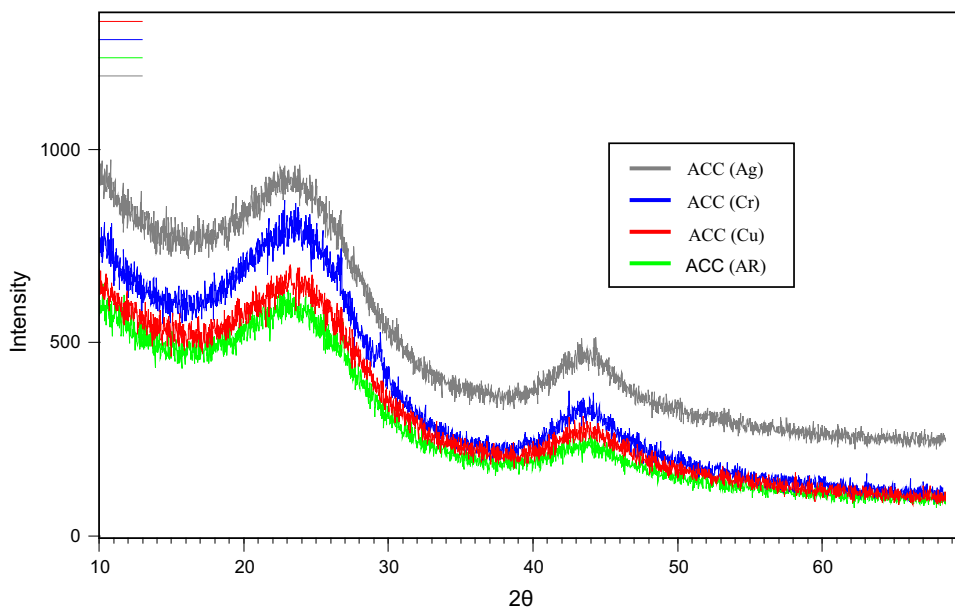


Table 6 Structural parameters of as-received and metal impregnated activated carbons deduced from XRD studies

Carbon sample	2θ ~ 23°				2θ ~ 43°		
	d ₀₀₂ (nm)	L _a (nm)	L _c (nm)	N _p	d ₁₀ (nm)	L _a (nm)	L _c (nm)
As-received	0.382	1.178	0.576	1.50	0.208	4.34	1.676
Cr-impregnated	0.376	1.181	0.612	1.63	0.204	4.37	1.682
Cu-impregnated	0.378	1.186	0.587	1.55	0.207	4.38	1.684
Ag-impregnated	0.377	1.184	0.607	1.61	0.205	4.39	1.681

carbons, 29 % in Cu-impregnated and 27 % in Ag-impregnated carbons. A similar trend can be seen in the DTG curves present three exotherms (peaks): a first one is from 45 to 160 °C, a second one from 200 to 600 °C and a third one is above 700 °C. The first peak is due to desorption or removal of adsorbed water. The peaks at temperatures around 200 °C are due to the decomposition or removal of surface oxygen containing functional groups present on the carbon surface. As mentioned earlier, it is well documented that CO₂ would be released at 200–600 °C because of the decomposition of carboxyl and lactone groups while CO would be released between 650 and 950 °C due to decomposition of carbonyl, phenol and quinone groups present on the carbon surface (Bansal et al. 1988). In case of metal impregnated activated carbons,

third one is more pronounced as compared to as-received ACC sample due to decomposition of metal oxides in addition to carbon–oxygen surface groups.

3.4.2 Adsorption isotherms on metal impregnated carbons

The adsorption isotherms of pyridine on ACC before and after impregnation with Cu²⁺, Ag⁺ and Cr⁶⁺ ions are shown in Fig. 10. The adsorption isotherms show that loading with Ag⁺ and Cu²⁺ increases the adsorption compared with the unloaded sample while loading with Cr⁶⁺ decreases the adsorption. The increase in adsorption of pyridine is maximum in case of Cu-impregnation and minimum in case of impregnation by Cr. This variation in the adsorption of pyridine on the activated carbon surface

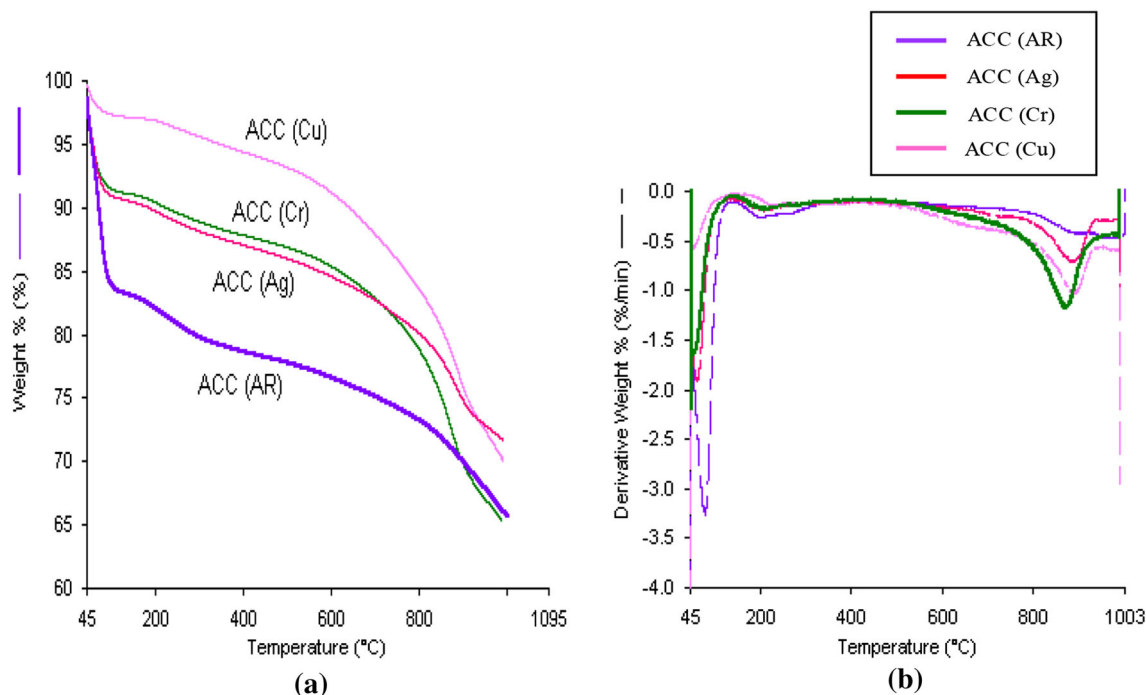


Fig. 9 a TG and b DTG curves for as-received and impregnated ACC samples (Color figure online)

on impregnation with metal ions can be explained on the basis of hard and soft acid base (HSAB) principle (Alfarrara et al. 2004; Yu et al. 2006). This principle states that hard acids prefer to bond to hard bases and soft acids to soft bases. According to Pearson classification (Pearson 1963), Ag^+ ion belongs to soft acid group while the Cr^{6+} ions belongs to hard acid. The Cu^{2+} ion belongs to borderline acids. Similarly pyridine is a borderline base. It has been observed in the present studies that the adsorption of pyridine increases on the Cu and Ag-impregnated carbon while it decreases in the case of the Cr-impregnated carbon, the increase being maximum in the case of Cu-impregnated carbon. Generally, it is seen that as the hard bases prefer to bond with hard acids and soft go with soft bases, the borderline bases generally bond with the borderline acids. This can explain a maximum increase in the adsorption of borderline base pyridine on the borderline Cu^{2+} ion impregnated carbon.

3.4.3 Desorption studies on metal impregnated carbons

The desorption of pyridine vapors has been studied on metal impregnated ACC samples. The adsorption–desorption isotherms are shown in Figs. 11, 12 and 13. The adsorption–desorption isotherms show that sorption–desorption branches do not meet even at zero relative vapor pressure. This indicates that a certain amount of pyridine vapors is held at the surface of these impregnated carbons so firmly that it can not be desorbed even when the system

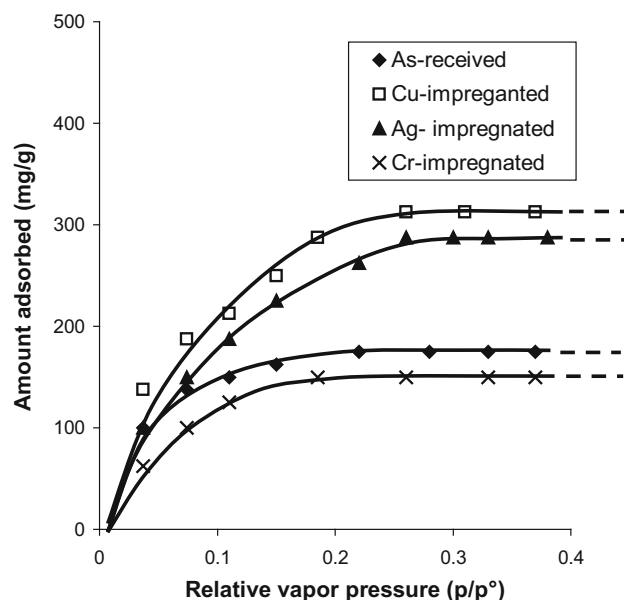


Fig. 10 Adsorption isotherms of pyridine vapors on ACC sample before and after impregnation

is evacuated to constant weight at 303 K which is the temperature of adsorption. This amount may be regarded as irreversibly adsorbed or fixed at the metal sites on the carbon surface by some mechanism involving chemisorption or other specific interactions or both, since physisorbed vapors can usually be desorbed readily at the temperature at which they were originally adsorbed.

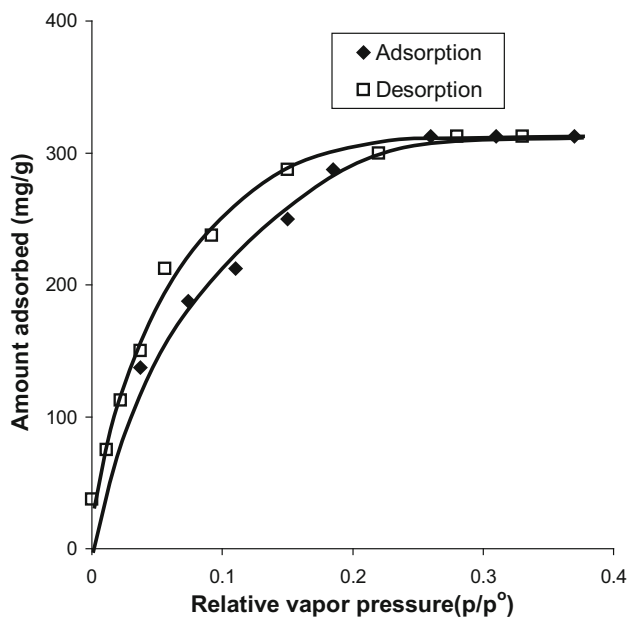


Fig. 11 Adsorption–desorption isotherms of pyridine vapors on Cu-impregnated ACC sample

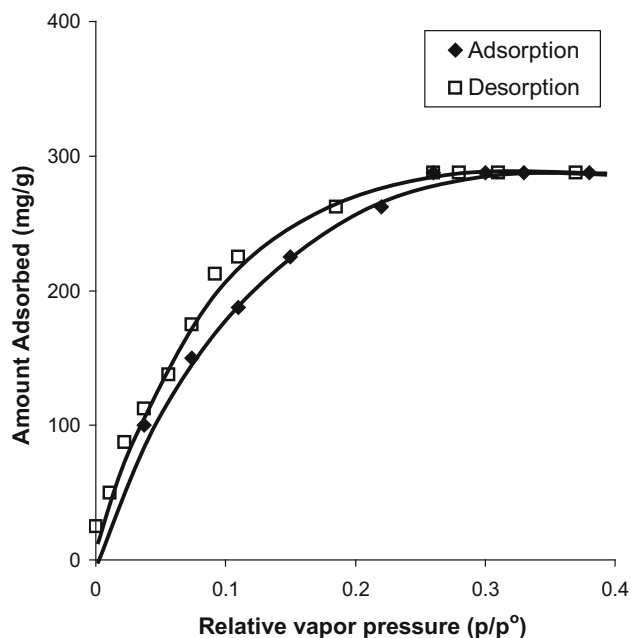


Fig. 12 Adsorption–desorption isotherms of pyridine vapors on Ag-impregnated ACC sample

Furthermore, this amount increases in the order: Cr-impregnated < Ag-impregnated < Cu-impregnated ACC samples. This trend further supports the fact that the interaction of pyridine vapors is maximum for Cu-impregnated ACC samples and minimum for Cr-impregnated as explained earlier on the basis of Hard-Soft acid base interactions.

3.5 Adsorption kinetics

The transport of gases and vapors into an activated carbon surface is a complex process. Consequently, there is only limited information available in the literature relating to the adsorption kinetics. It is likely that processes such as surface diffusion, diffusion in micropores and the chemical interactions with the carbon–oxygen surface groups could all make significant contributions towards adsorption on activated carbons. Thus keeping in mind the pore size distribution in activated carbons and the existence of different types of carbon–oxygen groups on the carbon surface, which make the carbon surface heterogeneous, the modeling of the kinetic process is quite difficult. The two more simple approaches to process the kinetic data could be to use either the Fick’s diffusion laws for homogeneous materials or to describe the process by phenomenological models. Since the activated carbons have heterogeneous surfaces, the assumption of the Fick’s diffusion law that the diffusion coefficient is constant is not valid in this case. The kinetic data, therefore, has been analysed using the empirical and phenomenological models.

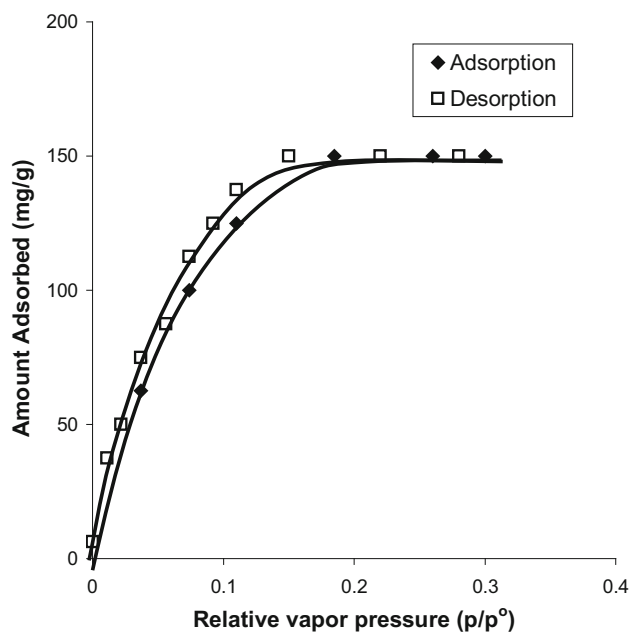


Fig. 13 Adsorption–desorption isotherms of pyridine vapors on Cr-impregnated ACC sample

3.5.1 Empirical diffusion model

Assuming that the surface concentration of a vapor is constant and that the diffusion is controlled by the concentration gradient through the particle, the kinetic of diffusion can be expressed (LaCava et al. 1989) by the empirical diffusion equation.

$$\frac{M_t}{M_e} = Kt^n,$$

where M_t is the vapor uptake at time t , M_e is the equilibrium vapor uptake, K is adsorbate-adsorbent interaction coefficient and n is the diffusional exponent. The diffusional exponent n and the interaction coefficient K can be evaluated from the linear plot of $\ln(M_t/M_e)$ against $\ln t$. When the value of $n = 0.5$ or less than 0.5 , the diffusion mechanism is Fickian (Chagger et al. 1995; Foley et al. 1997).

3.5.2 Linear driving force (LDF) mass transfer model

The kinetics of vapor adsorption may also be described by the following phenomenological model (Chagger et al. 1995) which is equivalent to a linear driving force model and can be represented as

$$\frac{M_t}{M_e} = 1 - e^{-kt},$$

where M_t and M_e are respectively the uptakes at any time t and at equilibrium and k is the rate constant. In this case, a plot of $\ln(1 - M_t/M_e)$ against time gives a straight line of gradient k .

3.5.3 Interpretation of the kinetic models

The diffusional exponent n and the interaction coefficient K have been evaluated from the linear plot of $\ln(M_t/M_e)$ against $\ln t$. The value of n is always greater than 0.5 in the case of all adsorbate-adsorbent combinations (cf. Table 7). This indicates that the adsorption of pyridine does not involve Fickian diffusion but may be considered as a pseudo first order mass transfer process between the vapor phase and the adsorption sites.

The values of K are considerably larger on the oxidized and as-received ACC samples compared with the value on 950° -degassed samples (cf. Table 7). It has been shown earlier that the oxidized and as-received ACC samples are associated with appreciable amounts of the carbon–oxygen surface groups which render the carbon surface polar in character. The molecules of pyridine are also polar in character and can involve into polar-polar adsorbate-adsorbent interactions. The values of K are significantly smaller for 950° -degassed carbon sample for pyridine. This indicates that the adsorption of polar pyridine molecules on the nonpolar 950° -degassed ACC sample, which is almost completely free of any carbon–oxygen surface groups, involves mainly dispersive interactions, the polar-polar interactions being of smaller value.

In this paper, as a first approximation, we have tried to calculate the contribution of polar-polar and dispersive

interactions by dividing the interaction coefficient (K) between the different contributions. As stated earlier that 950° -degassed ACC sample involves dispersive interactions only, therefore we can assume that the value of the interaction coefficient ($K = 3.2 \times 10^{-2}$) for adsorption of pyridine on the 950° -degassed carbon sample as the contribution of the dispersive interactions towards the interaction coefficient. Now, the contribution of polar interactions towards the interaction coefficient will be $(6.4 \times 10^{-2} - 3.2 \times 10^{-2} = 3.2 \times 10^{-2})$ and $(8.2 \times 10^{-2} - 3.2 \times 10^{-2} = 5.0 \times 10^{-2})$ respectively for the adsorption of pyridine on the as-received and oxidized carbon samples. For 400° and 650° -degassed, the contribution is $(7.4 \times 10^{-2} - 3.2 \times 10^{-2} = 4.2 \times 10^{-2})$ and $(3.9 \times 10^{-2} - 3.2 \times 10^{-2} = 0.7 \times 10^{-2})$ respectively. It is calculated that for pyridine, the polar interactions contribute about 50 % in case of as-received and 61 % in case of nitric acid oxidized samples which has larger amount of carbon–oxygen surface groups compared with as received ACC sample. In case of 400° -degassed and 650° -degassed, the contribution is 56 and 18 % respectively. As mentioned earlier, the presence of oxygen in the carbons will reduce the dispersive interactions by decreasing the electron density due to localization or withdrawal of electrons in the graphene layers while it will enhance the polar interactions. This indicates that dispersive interactions are less important in case of nitric acid oxidised samples while these play major role in case of 650° -degassed and 950° -degassed samples which have smaller amount of carbon–oxygen surface functional group. Furthermore, for as-received samples, both types of interactions contribute equally.

For the impregnated carbon samples, the value of K decreases in the order: Cu-impregnated > Ag-impregnated > Cr-impregnated ACC samples in case of pyridine. These values are included in the Table 7. These trends are based on the acid–base interactions of between the adsorbate and adsorbent. As mentioned earlier, Cu-impregnated ACC has greater affinity for pyridine.

Table 7 Kinetic Parameters for adsorption of pyridine vapors on different ACC samples

Carbon sample	n	K	E_a (kJ/mol)
As-received	0.88	6.4×10^{-2}	36.3
HNO ₃ -oxidised	0.90	8.1×10^{-2}	46.5
400° -degassed	0.91	7.4×10^{-2}	43.2
650° -degassed	0.95	3.9×10^{-2}	27.7
950° -degassed	0.96	3.2×10^{-2}	23.4
Cu-impregnated	0.83	7.8×10^{-2}	56.4
Cr-impregnated	0.87	6.0×10^{-2}	30.6
Ag-impregnated	0.94	7.2×10^{-2}	44.3

The values of rate constants k_1 , k_2 and k_3 at the three temperatures (293, 303 and 313 K) were determined from the linear plots of $\ln(1 - M_t/M_e)$ against time and these have been used to calculate the activation energies of adsorption (E_a) using Arrhenius plots. The activation energies for the adsorption of pyridine on as-received, nitric acid oxidized and 950°-degassed ACC samples are presented in Table 7. It is seen that the activation energy values for the adsorption of pyridine are quite large for the as-received and oxidized carbon samples. As the pyridine is polar molecule, it appears that the adsorption of these molecules involves two different interactions: the polar-polar interactions between the polar adsorbate molecules and the polar carbon–oxygen surface groups and the dispersive interactions. The activation energies of adsorption are in the domain of physisorption indicating that the adsorption is not chemical in nature and may involve the formation of quasichemical weak hydrogen bonds. This receives support from the smaller activation energy values for the adsorption of pyridine in the case of the 950°-degassed ACC sample which is almost completely free of any carbon–oxygen surface groups.

For impregnated carbons, the activation energies decrease in the order: Cu-impregnated > Ag-impregnated > Cr-impregnated ACC samples in case of pyridine. These trends are consistent with the interactions of these molecules with the metal impregnated activated carbons, as has been indicated earlier from the values of interaction coefficient K (calculated from the empirical diffusion model) for different adsorbent-adsorbate systems.

3.6 Isothermic enthalpy of adsorption

The isosteric enthalpies of adsorption for pyridine on the as-received and modified ACC samples were calculated from the adsorption isotherms at two temperatures of 303 and 313 K using the integrated form of the Clausius–Clayperon equation.

$$\left(\ln \frac{p_1}{p_2}\right)_{n_a} = \frac{-\Delta H}{R} \left(\frac{T_2 - T_1}{T_1 T_2}\right),$$

$$-\Delta H = q_{st}.$$

The isosteric enthalpies of adsorption at different surface coverages for different adsorbate-adsorbent systems are shown in Figs. 14 and 15.

It is seen that the zero surface coverage q_{st} decreases in the order: oxidized > as-received > 950°-degassed ACC samples, the value varying between 137 and 105 kJ/mol. This is due to the decreasing heterogeneity of the carbon surface (Al-Muhtaseb and Ritter 1999) which is due to the presence of carbon–oxygen surface groups at certain specific sites. It is also seen that q_{st} initially decreases and then increases with an increase in the surface coverage. As

adsorption proceeds, the influence of surface heterogeneity decreases and the contribution of lateral interactions is not large enough at intermediate θ values. These factors tend to decrease q_{st} at lower θ values. The lateral interactions become significant only at higher surface coverages ($\theta > 0.5$) and result in an increase in q_{st} . Figure 14 shows that at the minimal coverage of about 0.025, pyridine

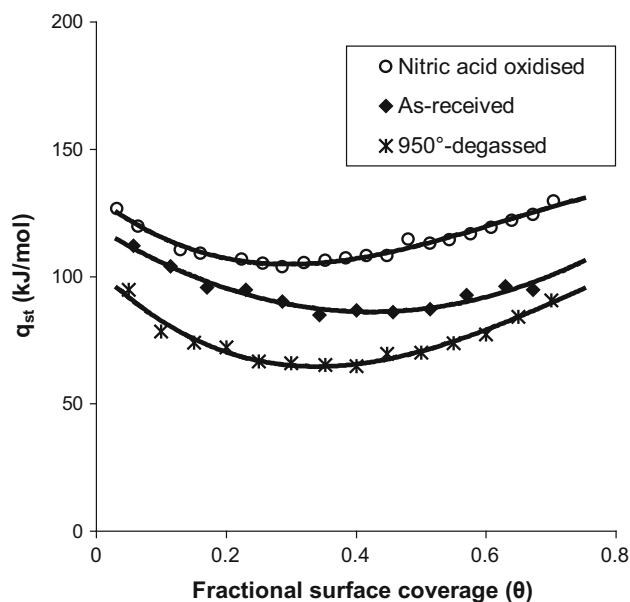


Fig. 14 Variation of isosteric enthalpy of adsorption with fractional surface coverage for the adsorption of pyridine vapors on different ACC samples

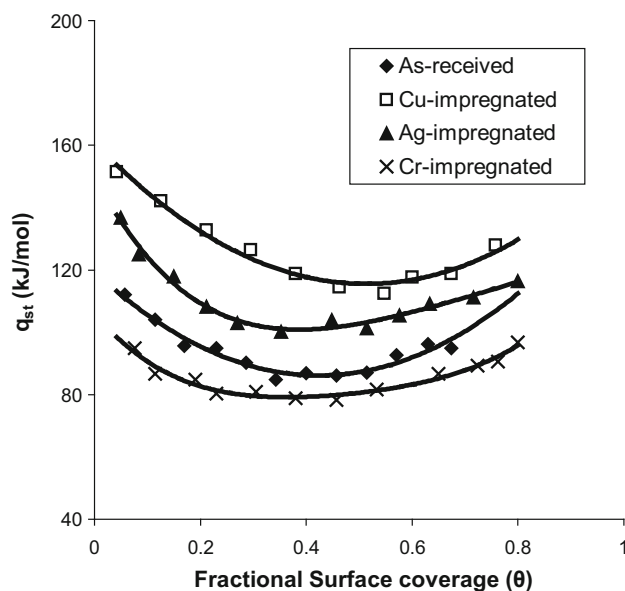
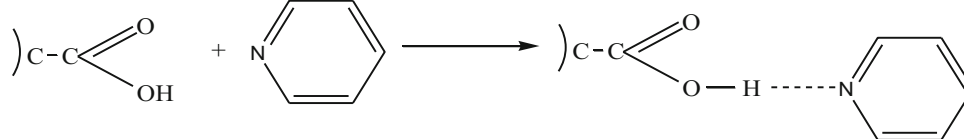


Fig. 15 Variation of isosteric enthalpy of adsorption with fractional surface coverage for the adsorption of pyridine vapors on ACC after impregnation

molecules occupy sites on as-received ACC sample whose energy is more than 122 kJ/mol in magnitude (the adsorption energy is negative). This means that all the sites whose adsorption energy is less than -122 kJ/mol are occupied by adsorbed molecules at the above coverage. These are the strongest sites on the carbon surface being characterized by lower magnitudes of adsorption energy. Similar trends were observed for the adsorption of pyridine on silica gel (Bakaev et al. 2007). If the coverage increases, the vacant sites are occupied by the newly arrived molecules. This can explain a monotonous decrease in the isosteric enthalpy of adsorption on a heterogeneous surface as a function of surface coverage.

compound polar in character. In addition the ring structure in these compounds has Π electrons which can also interact. Similarly activated carbons are invariably associated with acidic carbon–oxygen surface which make the carbon surface polar. The activated carbons also have graphene layers which contain Π electrons. Thus the adsorption of pyridine on activated carbons shall involve dispersive interactions between the Π electrons of the ring with Π electrons of the graphene layers as well as the polar-polar adsorbate-adsorbent interactions. The polar adsorbate-adsorbent interactions which may involve hydrogen bonding between the carbon–oxygen groups on the carbon surface and the nitrogen of pyridine can be represented as:

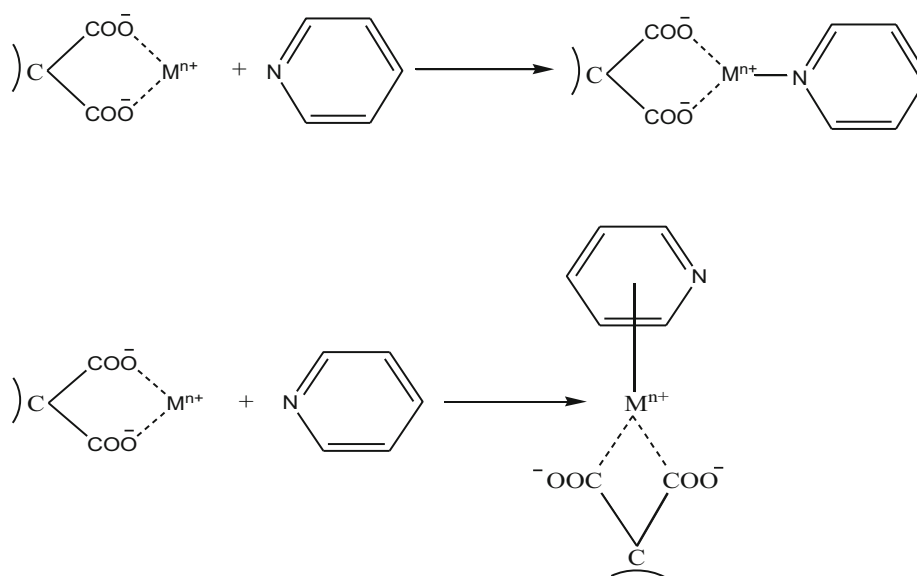


For the adsorption of pyridine on impregnated carbons, the zero surface coverage q_{st} decreases in the order: Cu-impregnated > Ag-impregnated > As-received > Cr-impregnated ACC samples (Fig. 15). These trends are based on the adsorption affinity of pyridine for these metal impregnated carbons. It might be assumed that pyridine act as Lewis base and coordinate with metal vacancies by utilizing the free electrons. The higher values of q_{st} for activated carbon impregnated with Cu and Ag metals may be due to a stronger interaction of the adsorbate molecules with metal vacancies present on the active carbon surface. The extent of coordination of adsorbate molecules with metal sites depends upon the acidic character of the metal.

3.7 Mechanism of adsorption

Pyridine has a six membered ring structure with a nitrogen atom as part of the ring. This heteroatom renders this

In the case of metal impregnated samples, the metals located in the pore entrances can act as active centers so that pyridine molecules can position themselves parallel or perpendicular to the surface depending on the type of nitrogen-metal interactions. It has been suggested that pyridine can interact with metals either via donation of a lone pair of electrons which is considered to be a direct N-metal bond or via delocalized electrons of the aromatic ring where a Π -type complex with the metals is formed. The latter arrangement should lead to a parallel location of pyridine molecules on the surface provided that the pore geometry and size allow it. These interactions for the adsorption of pyridine can be represented as:



4 Conclusions

Adsorption of pyridine vapors on activated carbons is influenced considerably by the nature and amount of carbon–oxygen functional groups as well as metals dispersed on carbon surface. The adsorption increases on oxidation due to the formation of carbon–oxygen surface groups. When these surface groups are gradually removed on degassing at increasing temperatures, the adsorption decreases. Loading Ag^+ and Cu^{2+} ions on ACC sample increased the adsorption of pyridine vapors in comparison with the unloaded ACC sample while loading of Cr^{6+} ions on ACC decreased the adsorption of these vapors. This has been attributed to the variation of the nature of soft and hard acid on the activated carbon surface. These interactions were further supported by the desorption studies on metal impregnated carbons. The kinetic data analysed using empirical diffusion model and the linear driving force mass transfer model indicates that the adsorption does not involve Fickian diffusion but may be considered as a first order mass transfer process. The trends in isosteric heats of adsorption for modified and unmodified ACC indicate the effect of both surface heterogeneity and lateral interactions. As pyridine is a polar molecule, it appears that the adsorption involves two different interactions: the electrostatic (polar) adsorbate-adsorbent interactions and the dispersive interactions in the case of as-received and oxidized carbons and largely the dispersive interactions in the case of 950°-degassed sample. It has been observed that the polar interactions contribute to between 50 and 60 % for as-received and oxidized carbon samples. In case of metal impregnated carbons, the metals at the pore entrances can be the active centers and pyridine can interact with

the metals either via donation of a lone pair of electrons (N-metal bond) or via delocalized electrons of the aromatic ring where a Π -type complex with the metals is formed.

Acknowledgments The authors acknowledge their thanks to Defence Research Development Organization, Delhi, CSIR and AICTE for the award of the research Grants. The authors are also thankful to HEG Ltd., Bhopal, India for the supply of ACC and SAC, the Ashland Petroleum Company, USA for the supply of ACF-307 and Norit N.V. Netherlands for the supply of GAC-R and GAC-1240.

References

- Agency for Toxic Substances and Disease Registry (ATSDR) and National Center for Environmental Health. 2008. Public Health Statement for Pyridine. Sidney Draggan (Topic Editor)
- Agency for Toxic Substances and Disease Registry (ATSDR): Toxicological Profile for Pyridine. U.S. Department of Health and Human Services, Public Health Service, Atlanta (1992)
- Alfarrara, A., Frackowiak, E., Beguin, F.: The HSAB concept as a means to interpret the adsorption of metal ions onto activated carbons. *Appl. Surf. Sci.* **228**, 84–92 (2004)
- Al-Muhtaseb, S.A., Ritter, J.A.: Roles of surface heterogeneity and lateral interactions on the isosteric heat of adsorption and adsorbed phase heat capacity. *J. Phys. Chem. B.* **103**, 2467–2479 (1999)
- Attia, A.A.: Some surface properties of activated carbons prepared by gasification with different gases. *Adsorpt. Sci. Technol.* **15**, 707–715 (1997)
- Bakaev, V.A., Bakaeva, T.I., Pantano, C.G.: On inverse adsorption chromatography. 2. Determination of isotherms and heats of adsorption as well as energy distributions of adsorption sites. *J. Phys. Chem. C* **111**, 7473–7486 (2007)
- Bansal, R.C., Bhatia, N., Dhama, T.L.: Surface characteristics and surface behavior of polymer carbons IV. Adsorption isotherms of organic vapors. *Carbon* **18**, 137–145 (1980)
- Bansal, R.C., Bhatia, N., Dhama, T.L.: Surface characteristics and surface behaviour of polymer carbons III. Surface acidity of polymer carbons. *Carbon* **16**, 65–68 (1978)

- Bansal, R.C., Donnet, J.B., Stoeckli, F.: *Active Carbon*. Marcel Dekker, New York (1988)
- Carrott, P.J.M., Nabais, J.M.V., Ribeiro Carrott, M.M.L., Pajares, J.A.: Preparation of activated carbon fibres from acrylic textile fibres. *Carbon* **39**, 1543–1555 (2001)
- Chagger, H.K., Ndaji, F.E., Sykes, M.L., Thomas, K.M.: Kinetics of adsorption and diffusional characteristics of carbon molecular sieves. *Carbon* **33**, 1405–1411 (1995)
- Chen, H.K., Miura, K., Li, W., Li, B.: Pyridine adsorption isotherms of several coals and factors influencing the coal adsorption behavior. *Ranliao Huaxue Xuebao* **32**, 135–139 (2004)
- El-Nabarawy, T.H., Petro, N.S.H., Abdel-Aziz, S.: Adsorption characteristics of coal based activated carbons. II. Adsorption of water vapors, pyridine, benzene. *Adsorpt. Sci. Technol.* **15**, 47–58 (1997)
- Foley, N.J., Thomas, K.M., Forshaw, P.L., Stanton, D., Norman, P.R.: Kinetics of water vapor adsorption on activated carbon. *Langmuir* **13**, 2083–2089 (1997)
- LaCava, A.I., Koss, V.A., Wickens, D.: Non-Fickian adsorption rate behaviour of some carbon molecular sieves. I. Slit-potential rate model. *Gas Sep. Purif.* **3**, 180–186 (1989)
- Muminov, S.Z.: Adsorption energy of microporous clay adsorbents in relation to polar adsorbates. *Uzb. Khim. Zh.* **1**, 76–81 (2003)
- Muminov, S.Z., Gulyamova, D.B.: Peculiarities of adsorption of some polar substances from vapor phase on a microporous clay adsorbent. *Colloid J.* **66**, 245–248 (2004)
- Muminov, S.Z., Gulyamova, D.B., Agzamkhodzhaev, A.A.: Adsorption of thiophene vapor on sodium and polyhydroxoaluminum montmorillonites. *Russ. J. Appl. Chem.* **77**, 376–379 (2004)
- Pearson, R.G.: Hard and soft acids and bases. *J. Am. Chem. Soc.* **85**, 3533–3539 (1963)
- Puri, B.R., Bansal, R.C.: Studies in surface chemistry of carbon blacks. I. High temperature evacuations. *Carbon* **1**, 451–456 (1964)
- Puri, B.R., Sharma, S.K.: Surface acidity of carbons. *Indian J. Chem.* **8**, 1119–1122 (1970)
- Short, M.A., Walker Jr, P.L.: Measurement of interlayer spacing and crystal sizes in turbostratic carbons. *Carbon* **1**, 3–9 (1963)
- Yu, M., Li, Z., Xia, Q., Xi, H.: Effects of different metal ions loaded onto activated carbon on adsorption of benzothiophene. *Huagong Xuebao* **57**, 1943–1948 (2006)
- Yuzak, Y., Fletcher, A.J., Thomas, K.M.: The compensation effect for the kinetics of adsorption/desorption of gases/vapours on microporous carbons, *Carbon' 01*, An International Conference on Carbon, Lexington, KY, United States, 14–19 July (2001) 1362–1363